RSC Advances

PAPER

View Article Online
View Journal | View Issue

Cite this: *RSC Adv.*, 2021, **11**, 19924

Tagetes erecta as an organic precursor: synthesis of highly fluorescent CQDs for the micromolar tracing of ferric ions in human blood serum†

Pinky Sagar,[a] Gopal Krishna Gupta,[b] Monika Srivastava,[c] Amit Srivastava[b] and S. K. Srivastava *[a]

Received 27th February 2021
Accepted 24th May 2021

DOI: 10.1039/d1ra01571k

rsc.li/rsc-advances

The present article illustrates the green synthesis of novel carbon quantum dots (CQDs) from biomass *viz.* *Tagetes erecta* (TE), and subsequently fabrication of a metal ion probe for the sensing of Fe^{3+} in real samples. TE-derived CQDs (TE-CQDs) have been synthesized by a facile, eco-friendly, bottom-up hydrothermal approach using TE as a carbon source. The successful synthesis and proper phase formation of the envisaged material has been confirmed by various characterization techniques (Raman, XRD, XPS, TEM, and EDS). Notably, the green synthesized TE-CQDs show biocompatibility, good solubility in aqueous media, and non-toxicity. The as-synthesized TE-CQDs show an intense photoluminescence peak at 425 nm and exhibit excitation dependent photoluminescence behavior. The proposed TE-CQD-based probe offers a remarkable fluorescence (FL) quenching for Fe^{3+} with high selectivity ($K_q \sim 10.022 \times 10^{13}$ M^{-1} s^{-1}) and a sensitive/rapid response in a linear concentration range 0–90 μM (regression coefficient $R^2 \sim 0.99$) for the detection of Fe^{3+}. The limit of detection (LOD) of the probe for Fe^{3+} has been found as 0.37 μM in the standard solution. It has further been applied for the detection of Fe^{3+} in real samples (human blood serum) and displays good performance with LOD ~ 0.36 μM. The proposed TE-CQD-based ion sensing probe has potential prospects to be used effectively in biological studies and clinical diagnosis.

1. Introduction

Iron is one of the most abundant elements in the earth's crust and essential for numerous metabolic activities of humans including DNA synthesis, facilitation of electron transfer, and transportation of oxygen.[1–4] Deficiency of iron causes the serious disease anemia.[5] However, over-accumulation of iron leads to heart damage, Parkinson's disease, liver, endocrine organ failure, *etc.*[4] Arumugham T. *et al.* and others have documented that an excess of iron produces free radicals throughout the redox cycling process in the presence of H_2O_2 and oxygen *via* Fenton reaction and turn severely affects the tissues, DNA, protein, and lipids by oxidative reactions.[1,4,6,7] Fe^{3+} and Fe^{2+} have been observed as two oxidation states of iron and are dynamically tweaked to one another. Subsequently, the precise and quantitative information of the trace level of Fe^{3+} is very essential as it plays a vital role in complex physiological and metabolic processes.[4] However, sensing of Fe^{3+} has been performed by many researchers, but in HBS based on CQDs probe through FL technique, have rarely been reported[5] so far.

CQDs, known as carbon dots/carbon nanoparticles have been an emerging class of innovative fluorescent materials due to their outstanding properties like tiny size (less than 10 nm), low toxicity, excellent emission tenability, chemical stability, temperature stability, high carrier mobility, biocompatibility, resistivity to photobleaching, cost-effectiveness, *etc.*[8–13] Moreover, owing to their environment friendliness in comparison to other chemical dyes and semiconductor QDs, superiority in photostability, ability in up and down-conversion, non-blinking FL emission, CQDs have been preferable for the sensing applications due to their FL quenching or enhancement occurrence. A wide spectrum of approaches has been developed for the synthesis of CQDs such as plasma treatment,[14] chemical ablation,[15] arc discharge,[16] acidic oxidation, electrochemical oxidation, hydrothermal carbonization,[12,17] microwave irradiation,[18] combustions (pyrolysis).[19] However, some reported methods involves tedious steps and mark harmfulness to the

[a]*Department of Physics, Institute of Science, Banaras Hindu University, Varanasi, India, 221005. E-mail: sanjay_itbhu@yahoo.com*

[b]*Department of Physics, TDPG College, VBS Purvanchal University, Jaunpur, India, 222001*

[c]*School of Materials Science and Technology, IIT (BHU) Varanasi, India, 221005*

† Electronic supplementary information (ESI) available: Comprises photoluminescence spectra of TE-CQDs at various excitation wavelengths, the optical excitation spectrum of TE-CQDs, images of TE-CQDs in presence and absence of Fe^{3+}, FT-IR spectrum of TE, binding affinity constant values against different interference, modified S–V plot for the sensing of Fe^{3+} in standard solution and HBS sample 1, linearity plot of the probe, FL quenching analysis for the HBS sample 2, TRPL study table and a brief study of the present work. See DOI: 10.1039/d1ra01571k

ecosystem such as polamine functionalization,[20] poly coupling reactions,[21] thiol–yne click reactions,[22] photo initiated raft,[23] thiol–ene click reaction,[24] azide–alkyne click reaction.[25] Li *et al.* have synthesized CQDs *via* hydrothermal approach using citric acid as a precursor followed by the addition of CTAB. It leads to cytotoxicity[26] and makes it non-suitable for biosensing applications.[27] The hydrothermal synthesis of CQDs has been one of the easy and outstanding approaches, and widely popular among the researchers due to its mild circumstances, large-scale production, deprived of strong acids, and purity of samples.[12] CQDs, as-synthesized through this approach has been extensively employed for different applications such as biosensors, therapeutic purposes, drug discovery, energy storage device, and so forth.[4,28,29]

Beyond troubling ambiguity with the selection of appropriate synthesis route, a true and big issue has been the preference of environment friendly and cost-effective precursor also. To find a way around, diverse precursors including green/biowaste/sustainable sources such as banana juice, coffee grounds, cellulose,[3,30] *Catharanthus roseus*,[7] pistachio shells,[31] waste paper,[32] ethylenediamine,[33] rice husk,[34] watermelon juice,[35] gelatine,[36] bamboo,[37] *etc.* have been used as rich carbon source replacing hazardous chemicals.[38,39] Serendipitously, we have found TE as an emerging precursor to synthesize the CQDs having excellent FL and biocompatibility. Notably, TE contains thiophenes, triterpenoids, flavonoids, carotenoids, oxycarotenoid, and xanthophylls chemical constituents which have worth therapeutic values such as non-cytotoxicity, antioxidant, antibacterial, antifungal, wound healing, *etc.*[40] The earlier studies suggest that the extraction of flower petals has been a rich source of pharmaceutically important ethanol and ethyl acetate, used in anticancer drugs against H460 lung cancer, $CaCO_2$ colon cancer lines, MCF-7 breast cancer lines.[41,42] Apart from the far-reaching range of the applications of TE, a recent report reveals the phytoremediation of lateritic soil polluted by heavy metal.[43] Maji *et al.* have studied the antibacterial properties and interaction of human serum albumin of TE leaves.[44]

Innumerable sensing probes using carbon-based materials for the detection of metal ions using electron paramagnetic resonance,[45] solution-gated graphene transistors (SGGT),[46] coupled plasma mass spectroscopy,[47] atomic absorption/emission spectroscopy,[48] colorimetry,[49] electrochemical detection,[50] *etc.*, have grabbed attention. But they are pricey, need complex instrument operation and sample pre-treatment along with long interval procedures.[46,49] However, the FL technique has emerged as one of the most pronounced techniques owing to its high accuracy, superficial handling, and no pre-cure of an analyte, which makes it a favourable option for several sensing applications.[51] Mohammed *et al.* have engineered an FL nanosensor based on B,N co-doped carbon nanodots for the successive and reliable determination of Fe^{3+}. The engineered sensor has shown its ability to detect Fe^{3+}, however, it also binds with Fe^{2+} simultaneously, which marks it inferior for selective detection.[9] Fan *et al.* designed an SGGT based on the functionalization with CQDs for the detection of Fe^{3+}.[46] Qian *et al.* have reported dual fluorescent sensors for the sensing of Fe^{3+} and Ag^{+}, which makes it vague for Fe^{3+}.[52] Among these methods, a sensitive, specific, simple operative and accurately gauging of Fe^{3+} status in real samples based on FL technique has hardly been discussed.[3,7,34] Henceforth, eco-friendly synthesis of materials with excellent optical properties and their FL based sensing applications for the rapid analysis of noteworthy biological samples has remained an emerging topic.

In the present study, a novel CQDs has been synthesized from an eco-friendly and sustainable TE as a carbon source for the very first time opting for a facile bottom-up "hydrothermal method" as a simplistic alternate for the pure, less than 10 nm-sized and large scale production. Besides the process does not involve any concentrated acids or strong reducing agents and surface passivation reagents. Furthermore, TE-CQDs have been characterized by the XRD, TEM, and Raman techniques and subsequently confirm the formation of CQDs with a good abundance of 4–6 nm sized particles. Moreover, the photophysical properties of TE-CQDs have also been investigated through UV-Visible, photoluminescence, and FT-IR spectroscopy. FT-IR studies reveal the presence of many active sites on the surface of TE-CQDs such as COOH, NH, and OH functional groups. The nanometer-sized TE-CQDs exhibit blue FL with UV-Visible light ($\lambda = 365$ nm). The FL quenching behaviour has also been investigated through the gradual addition of Fe^{3+} in DI water. The quenching process has been analyzed with Stern–Volmer (S–V) plot, modified S–V plot, and time-resolved photoluminescence (TRPL) spectra, which unveil the miscellaneous quenching *i.e.* static as well as dynamic quenching. However, the high value of the quenching constant ($K_q \sim 10.022 \times 10^{13}$ M^{-1} s^{-1}) indicates the selective and sensitive detection of Fe^{3+}. The lower LOD has been found as 0.37 μM in the standard solution under an optimized condition with linearity range 0–90 μM and regression coefficient $R^2 = 0.99$. Additionally, to validate the practical application, a similar experiment with HBS has been performed and elucidated an in-depth mechanism of FL quenching phenomenon in the existence of Fe^{3+}. Henceforth, the present study infers that the as-synthesized TE-CQDs have noteworthy sensing application competence and virtuous commercial prospective.

2. Experimental section

2.1. Reagents

TE was collected from the botanical garden of the BHU campus, Varanasi, India. Other chemical reagents were procured from Sigma Aldrich. For the dilution of the reagents required during synthesis, DI water was used. All the sensing measurements were done with DI water. The metal salts L-cysteine, D-glucose, glycine, creatinine, ascorbic acid, uric acid, and Tris HCl buffer were purchased from HiMedia, Merck, and Sigma Aldrich. Different kinds of metal salts were also prepared in DI water for optical sensing. For the real sample sensing, HBS samples were collected from Prakash Pathology, Varanasi, India.

2.2. Apparatus

The photophysical properties of TE-CQDs were characterized by UV-Visible absorption spectrophotometer (PerkinElmer, USA),

photoluminescence spectrophotometer (PerkinElmer, USA), and time-resolved photoluminescence spectrophotometer (TRPL, FLS920 Edinburgh, UK) using DI water as a solvent in quartz cuvettes of 1 cm optical path length. Raman spectroscopy was carried out on a Raman spectrometer (Renishaw, UK) equipped with a diode pump solid-state laser as a constant power source of 5 mW mm^{-2}. Fourier transform-infrared spectroscopy (FT-IR) was done on FT-IR spectrophotometer Varian Excalibur 3000, Palo Alto, CA using KBr as pellets ranging from wavenumber 400 cm^{-1} to 4000 cm^{-1}. XPS was recorded on XPS spectrophotometer, AMICUS, UK. All the measurements were repeated in triplicates for the determination of the elemental composition (at%). Transmission electron microscopy (TEM) and Energy Dispersive X-ray (EDX) observations were recorded on FEI Technai G2 F20-Twin (Swiss Republic) at an accelerating voltage of 300 kV on a carbon-coated copper grid. X-ray powder diffraction (XRD) pattern was recorded on Miniflex 600 X-Ray-Diffractometer (Cu-K_α radiation, $\lambda = 1.54056$ Å, and 3° min^{-1} scan rate) ranging 2θ from 5° to 70°.

2.3. Synthesis of TE-CQDs from TE

TE-CQDs were synthesized by one hand facile hydrothermal method using TE as a main reaction precursor. TE petals were washed thoroughly with DI water and allowed to dry at room temperature. Further, the TE petals were ground well in a pestle with the help of mortar. Next, 1.8719 g of TE powder was dissolved in 50 mL of 0.1 M HCl followed by ultrasonication for 30 min at room temperature. The as-received homogenous mixture was transferred to the stainless steel autoclave with Teflon vessel (100 mL capacity) and allowed to heat at 180 °C for 12 h as shown in Fig. 1. Further, it was kept to be cooled naturally to room temperature, the yellowish colloidal solution containing TE-CQDs was collected in a clean vessel and centrifuged further at 10 000 rpm for 30 min. The centrifuged solution was filtered to discard non-soluble/residual particles and kept safe for further characterizations and sensing measurements.

2.4. Sensing procedure of Fe^{3+}

To study the interaction of different metal ions/proteins, freshly prepared metal ion solutions have been separately added to a quartz cuvette containing TE-CQDs. Further, the variation in the FL intensity has been recorded with the peak wavelength ~425 nm at excitation wavelength 320 nm. After that interference study has been performed by adding 100 times higher concentration of different metal ions/proteins to the colloidal solution of TE-CQDs. Then, FL titration experiment based on quenching phenomena has been carried out by adding Fe^{3+} solution to the TE-CQDs.

2.5. Sensing procedure of HBS Fe^{3+}

Briefly, 20 μL of each HBS samples were taken into Eppendorf centrifuge tubes and diluted with 1 M Tris HCl buffer solution (pH = 7.4), separately and kept inside the refrigerator (4 °C) until use. However, the diluted solutions were used for the sensing of iron in HBS at room temperature.

3. Results and discussion

3.1. Characterizations of TE-CQDs

TE-CQDs in colloidal form, exhibit outstanding properties rendering their applications in various fields such as biosensing, optoelectronics, *etc.*[53,54] The UV-Visible spectrum has been recorded in quartz cuvettes (path length 1 cm) with the scanning wavelength range ~190 to 800 nm. The optical UV-

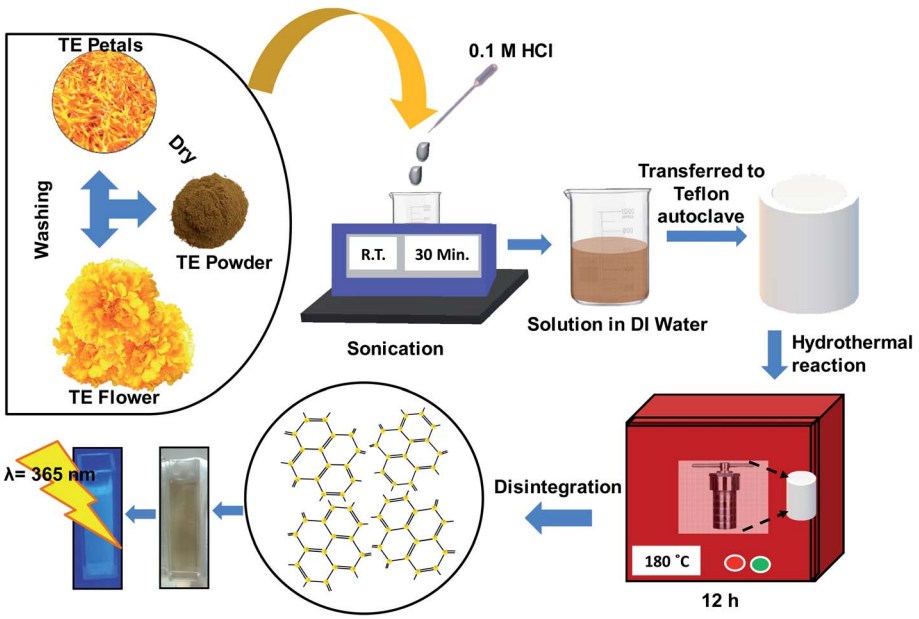

Fig. 1 Schematic representation of the synthesis of TE-CQDs by hydrothermal route.

Visible absorption spectrum of as-synthesized TE-CQDs reveals the appearance of an absorption band at 261 nm and an appendage owing to n–π* transition in C=O[39] and π–π* transition in the aromatic compounds[55,56] (Fig. 2a). The aqueous solution of as-synthesized TE-CQDs shows excellent blue FL, as depicted in Fig. 2a. To confirm this, the photoluminescence emission spectrum at different excitation wavelengths has been recorded in the region 240 nm to 370 nm, as shown in Fig. S1.† There has been a redshift which is a natural characteristic of a colloidal synthesis and may be attributed to the polydispersity of the QDs. However, as the excitation wavelength is increased, the FL intensity decreases and unveil the excitation-dependent properties of TE-CQDs[33,57] (Fig. S2a†). Further, the FL excitation spectra of TE-CQDs has been noted for $\lambda_{em} \sim 425$ nm with an obvious spectroscopic overlapping for $\lambda_{ex} \sim 320$ nm (Fig. S2b†).

As shown in Fig. 2b, to ascertain the chemical moieties present over the surface of the as-synthesized TE-CQDs, FT-IR analysis has been performed. Furthermore, FT-IR of a precursor (Fig. S3†) has also been carried out, as an indicator to optimize the synthesis criteria for TE-CQDs. The FT-IR spectra of TE-CQDs and its precursor exhibits absorption band at ~3322 cm^{-1}, 2930 cm^{-1}, 2849 cm^{-1}, 1734 cm^{-1}, 1707 cm^{-1}, 1567 cm^{-1}, 1015 cm^{-1}, and 831 cm^{-1} ascribes to O–H/N–H stretching, C–H bending, C–C/CH_2, COOH, C=O, C=C, C–O–C/C–N and O–O functional groups,[31,39,58] respectively. The presence of symmetric and asymmetric stretching of CH_2 reveals that the carbon quantum dots primarily consist of hydrocarbons. Furthermore, the existence of carboxyl and carbonyl functional groups (C=O and C=C) significantly indicates that the as-synthesized TE-CQDs possess graphitic structure. The absorption bands at 3305 cm^{-1}, 1734 cm^{-1}, and 1567 cm^{-1} correspond to its hydrophilic nature and excellent stability in water.[58,59]

Raman spectroscopy has been a well-known and effective technique to confirm the crystal quality and several layers in the as-synthesized 2D materials. Fig. 2c depicts the Raman spectra of the as-synthesized TE-CQDs. It consists of two characteristic peaks at 1353 cm^{-1} and 1577 cm^{-1} which correspond to the graphitic growth (G) and defect (D) bands.[60] The G-band attributes to E_{2g} (in-plane vibration of sp^2 bonded atoms) whereas the D-band owes to A_{1g} (out of plane vibration), for as-synthesized TE-CQDs. The Raman mode E_{2g} shows comparatively low intensity which might be due to the Rayleigh scattering or selection rules of the geometry whereas the high intensity of A_{1g} mode unveils the presence of oxygen-rich groups over the surface of TE-CQDs,[61] and are in good consistency with the FT-IR study.

The XRD pattern of as-synthesized TE-CQDs reveals a graphitic structure with good crystallinity. The XRD pattern exhibits two peaks at ~31° and ~45° corresponding to reflection planes (100) and (102) indicating the formation of graphitic TE-CQDs.[33,62] as can be seen in Fig. 2d. Furthermore, the peak at

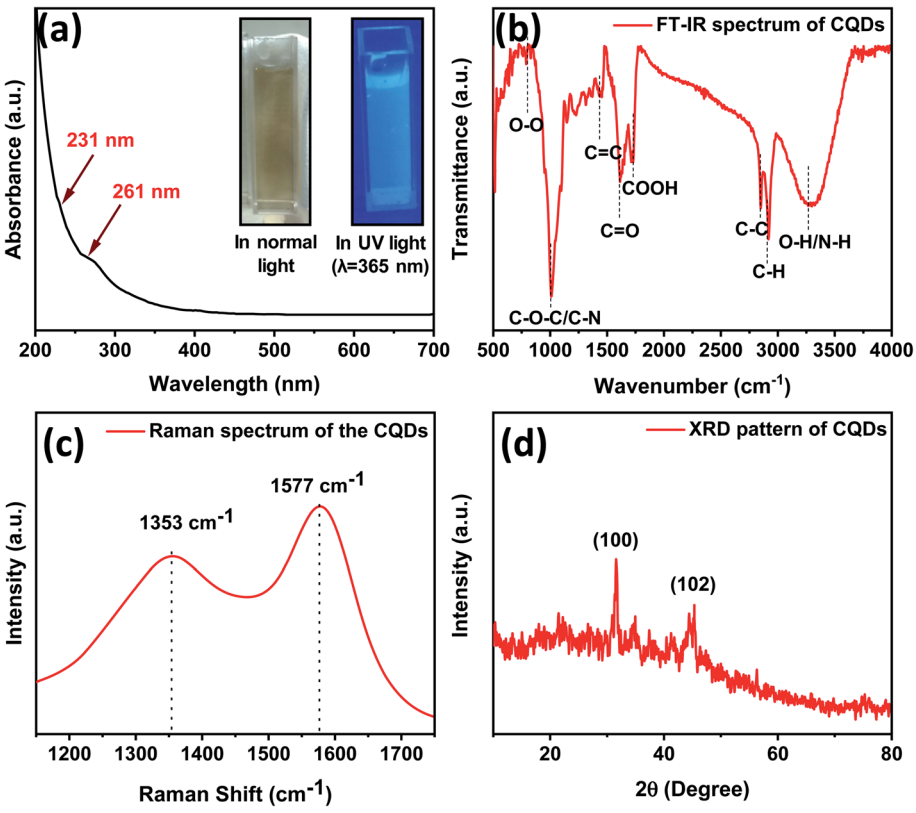

Fig. 2 (a) UV-Visible spectrum, inset: optical images of colloidal solution of TE-CQDs, and (b) FT-IR spectrum, (c) Raman spectrum and (d) XRD pattern of as-synthesized TE-CQDs.

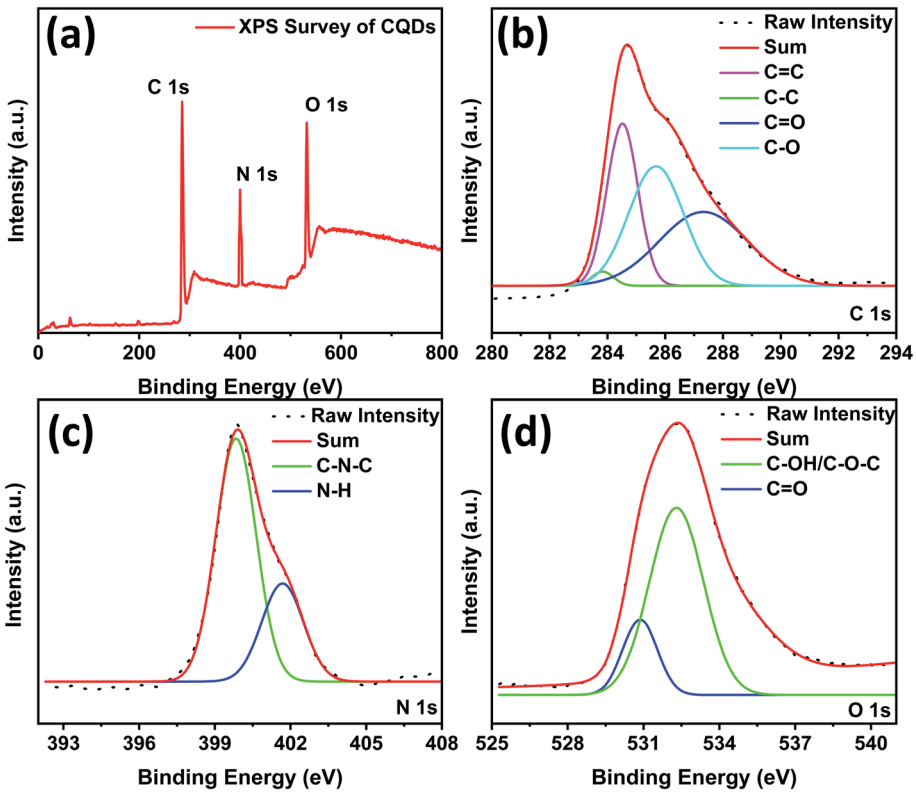

Fig. 3 (a) XPS survey, (b) C1s, (c) N1s and (d) O1s spectrum of synthesized TE-CQDs.

~23° may be due to the presence of an oxygen-containing functional group and is in accord with other research studies.[31]

XPS measurement has been carried out to elaborate the surface chemical compositions of the as-synthesized TE-CQDs sample. Fig. 3a depicts the presence of C1s, N1s, and O1s peaks correspond to compositions having an atomic percentage of ~82%, ~4%, and ~14%, respectively. C1s spectrum (Fig. 3b) reveals the presence of four distinct functional groups *i.e.* C–C (283.8 eV), C=C (284.5 eV), C–O (285.6 eV) and C=O (287.3 eV).[63,64] The N1s (Fig. 3c) peak corresponds to two different functional groups C–N–C (399.80) and N–H (401.69 eV).[9,64] The O1s spectrum (Fig. 3d) describes two peaks corresponding to C=O (530.81 eV) and C–OH/C–O–C (532.31 eV).[9,26,64] Hence, XPS reveals the XPS measurement reveals the presence of various functional groups present over the surface of TE-CQDs which has been well corroborated through FT-IR study too.

To get an insight into the structural morphology of the as-synthesized TE-CQDs, TEM investigations have been carried out. Fig. 4 represents the TEM micrograph of an as-synthesized sample which reveals the formation of spherical particles with an average diameter of 4.5–6.0 nm and predicts a good abundance of ~5 nm sized particles (Fig. 4a and c) and soluble in water. The lattice spacing (2.2 Å) has been observed through the Fig. 4d and directs the graphitic plane (100) in the as-synthesized TE-CQDs.[65] Also, the EDX profile infer a high wt% of the carbon in the as-synthesized sample, as shown in Fig. S4.†

3.2. Sensitive and selective sensing of Fe^{3+}

Functional groups containing oxygen-rich compounds over the surface of the as-synthesized TE-CQDs render its potential prospect in metal ion detection as it is easier to interact with metal cations for the formation of complex compounds. Henceforth, the as-synthesized TE-CQDs can be successfully applied for the sensing of anions, cations, and other hazardous chemicals by its turn-off FL effect as a probe. In selectivity experiment it has been found that our synthesized TE-CQDs are highly selective to Fe^{3+}. FL intensity has been quenched to 70% upon addition of Fe^{3+} while in case of metal ion/protein solutions (Zn^{2+}, Mg^{2+}, Na^{+}, K^{+}, Co^{2+}, Sn^{2+}, Cu^{2+}, Mn^{2+}, Ni^{2+}, Cd^{2+}, Pb^{2+}, Fe^{2+}, Cr^{2+}, L-cysteine, ascorbic acid, uric acid, glutathione, glycine, and creatinine), no obvious changes have been observed.

Furthermore, in the interference analysis of different metal ion/protein solutions, a separate fluorescent-based interference experiment has been carried out. In the process, the concentration (~0.2 mM) of different metal ions/proteins has been kept nearly 100 times higher than the Fe^{3+} solution. The study has been carried out with excitation wavelength ~320 nm and an intense peak at ~425 nm. With the addition of various metal ion/protein solutions, it has been observed that the FL intensity of as-synthesized TE-CQDs gets quenched nearly to ~10% only, while with Fe^{3+}, there has been complete disappearance of the FL. Fig. S5† depicts the optical representation leading to the quenching process of the FL of as-synthesized TE-CQDs with the addition of Fe^{3+}. The relative FL intensity plot has been

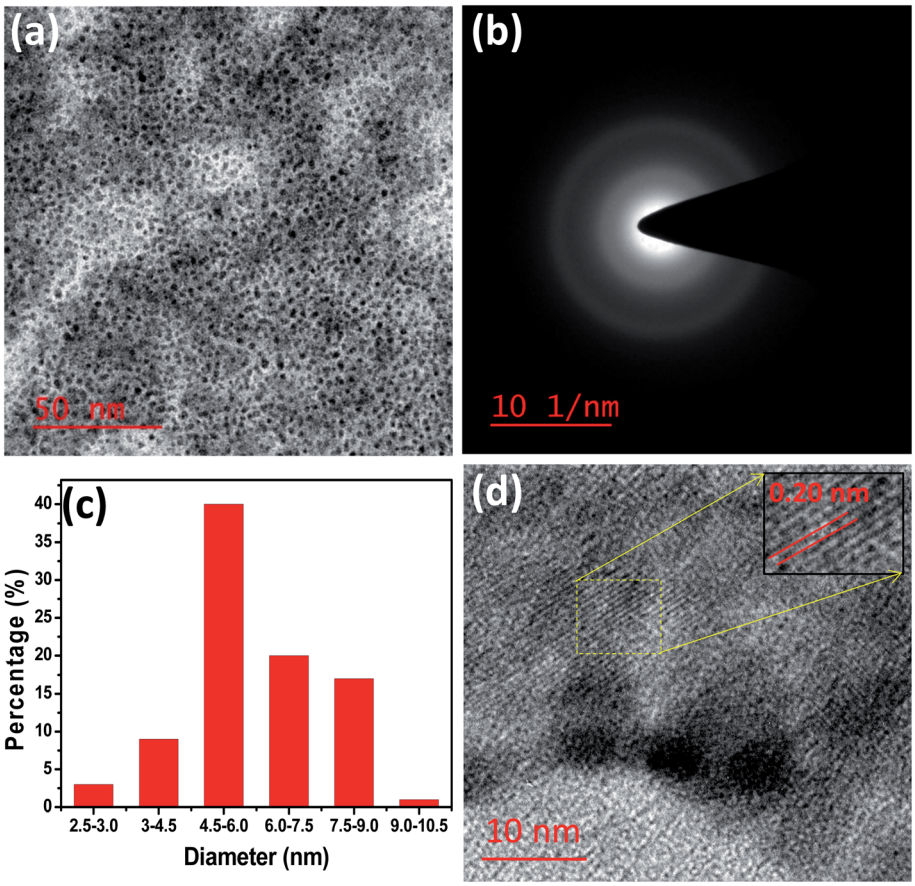

Fig. 4 (a) and (b) TEM images, (c) particle size profile, (d) HRTEM image indicating lattice fringes of as-synthesized TE-CQDs.

shown in Fig. 5 and the respective QP has been accessed through the equation:

$$\mathrm{QP} = \frac{(F_0 - F)}{F} \times 100\% \quad (1)$$

Here F_0 and F describe the FL intensities of TE-CQDs with and without Fe^{3+}, respectively.

Furthermore, to check the response of various metal ions/proteins on the FL intensity of TE-CQDs in presence of Fe^{3+}, an interference has been performed on TE-CQDs solution containing Fe^{3+}. There is no significant change that depicts a highly selective response of the proposed sensor towards the detection of Fe^{3+}. To check the sensitivity, an emission-based FL titration experiment has been performed. With a gradual addition of different concentrations (from 0 μM to 200 μM) of Fe^{3+} solution, the FL intensity of TE-CQDs quenches at 200 μM and further gets saturated (Fig. 6a). Notably, FL quenching by

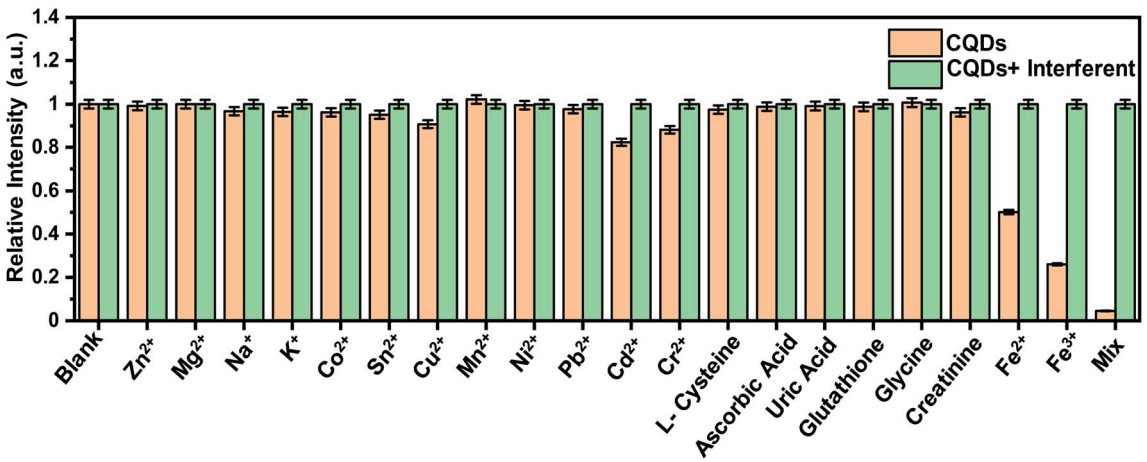

Fig. 5 Interference study of TE-CQDs for the sensing of Fe^{3+} in standard solution and HBS.

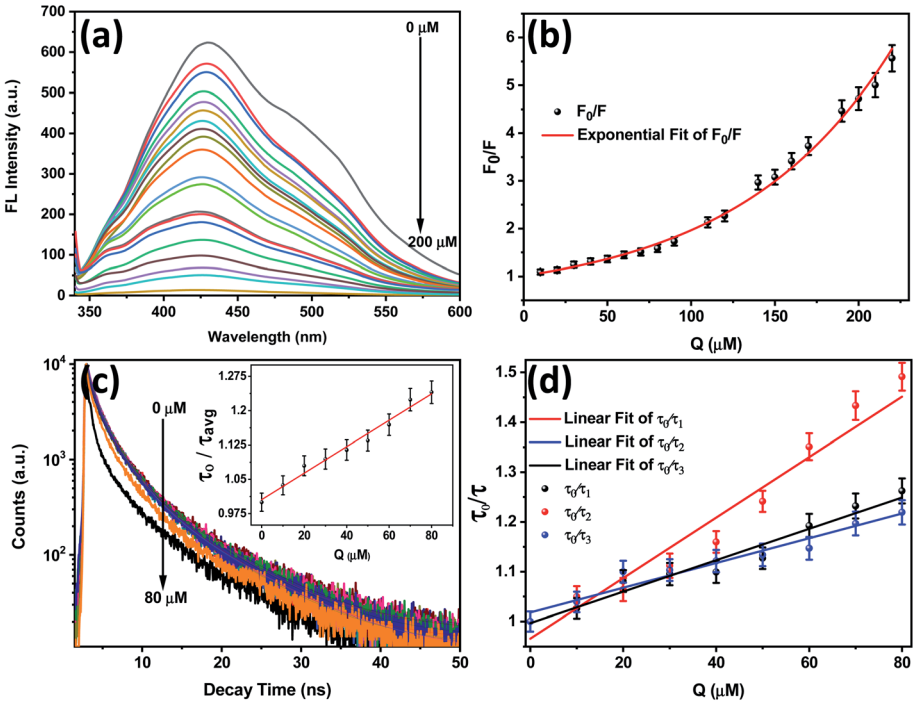

Fig. 6 (a) FL emission spectra upon gradual addition of Fe^{3+} concentration (at excitation wavelength $\lambda = 320$ nm), (b) S–V plot showing exponential quenching behaviour in FL intensity of TE-CQDs with the successive addition of Fe^{3+}, (c) TRPL spectra of TE-CQDs upon gradual addition of Fe^{3+} from 0 to 80 μM (inset: profile of average lifetime decay), and (d) calibration plot of lifetime decay for τ_1, τ_2, and τ_3.

Fe^{3+} can be seen by naked eyes in presence of UV lamp ($\lambda = 365$ nm) as shown in Fig. S5.†

3.3. Sensing of Fe^{3+} by TE-CQDs in standard solution

To understand characteristics of the FL quenching of as-synthesized TE-CQDs sample, with the gradual addition of Fe^{3+}, an S–V plot dealing with the variation of F_0/F with the concentration of Fe^{3+} (Q) has been drawn (Fig. 6b) by employing the equation:[4]

$$\frac{F_0}{F} = 1 + K_{S-V}(Q) \quad (2)$$

Here, F_0 and F represent the FL intensities of TE-CQDs with and without Fe^{3+} and the S–V quenching constant K_{S-V} entails the sensitivity of the fluorophore towards the quencher (Fe^{3+}) or the rate of FL quenching upon addition of Fe^{3+}. In the present study, the exponential fitting suggests that the FL quenching is non-linear and depicts the quenching phenomena as a complex one. Thus, the quenching of FL intensity can be attributed to a variety of processes which include dynamic and static quenching. When the fluorophores are excited, collides with some other molecule, and de-excites, the quenching is called dynamic or collisional quenching. On the other hand, some of the fluorophores make non-fluorescent complexes with the quencher in the ground state and does not involve any collision or diffusion process. This phenomenon leads to a static quenching.

So for a better understanding of the complex quenching phenomenon, a modified S–V plot has been (Fig. S6†) drawn following the equation:[66]

$$\frac{F_0}{\Delta F} = \frac{1}{f_a K_a(Q)} + \frac{1}{f_a} \quad (3)$$

Here ΔF, f_a, and K_a (Q) denote the difference of FL intensities in the absence and presence of the quencher, and S–V quenching constant for attainable quencher, respectively. Further, f_a and K_a have been extracted through a modified S–V plot as shown in Fig. S6.† The $f_a{}^{-1}$ and $(f_a K_a)^{-1}$ have been estimated as 0.598 and ~1.41 M, respectively, and thus demonstrate that most of the initial FL intensity has been approachable by the quencher. This suggests that nearly 42% of the maximum FL intensity gets quenched by the quencher if reaches the electron efficient hydroxyl group and form a non-fluorescent species $Fe(OH)_3$. Additionally, the quenching constant K_a has a value ~4.24×10^3 M^{-1} which is ~56.5% of the collision quenching phenomena derived constant and suggests a defined way of the quenching by quencher towards the TE-CQDs FL intensity.

Furthermore, to analyze the dynamic and static quenching processes, a quite sensitive technique TRPL spectroscopy, with and without successive addition of the quencher at excitation wavelength 320 nm assuming FL intensity peak at ~425 nm has been performed and shown in Fig. 6c. The average lifetime of as-synthesized TE-CQDs decays from ~2.83 ns to ~1.24 ns (inset of Fig. 6c). The TRPL decay investigation has been done using suitable software and the data has been found best fitted with the third-order exponential decay following the equation:[66]

$$y = A_1 \exp\left(-\frac{t}{\tau_1}\right) + A_2 \exp\left(-\frac{t}{\tau_2}\right) + A_3 \exp\left(-\frac{t}{\tau_3}\right) \quad (4)$$

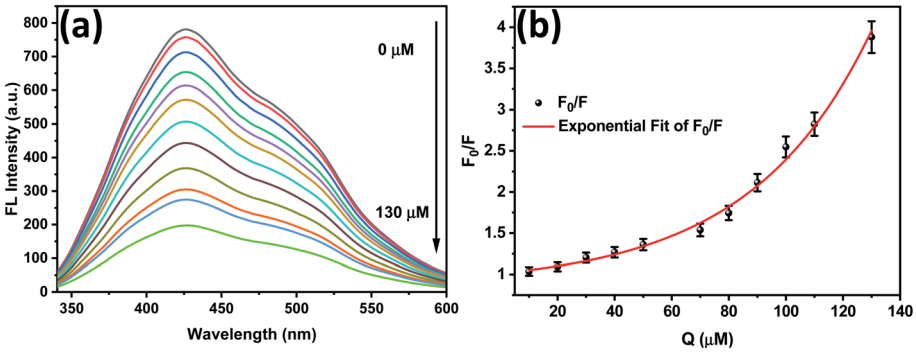

Fig. 7 (a) FL emission spectra with various concentration of Fe^{3+} in HBS sample 1 and (b) S–V plot showing exponential quenching of FL intensity of TE-CQDs.

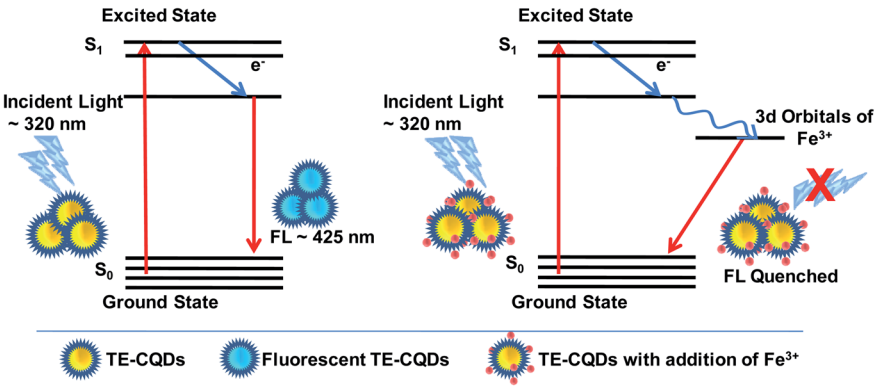

Fig. 8 Schematic illustration of FL quenching effect-based sensing of Fe^{3+} by the TE-CQDs as sensor.

It depicts that the FL quenching involves three types of quenching species[66] and in good agreement with S–V plot analysis. It has been observed that the lifetime τ_1 decays to ~1.47 ns from ~1.85 ns, τ_2 to ~0.42 ns from ~0.60 ns, and τ_3 to ~5.06 ns from ~6.05 ns. Its linear plot predicts that τ_1 and τ_3 decrease slow with the gradual addition of the metal ion solution (Fe^{3+}), as can be seen from the graph (Fig. 6d). The obtained results corresponding to the quenching have been represented in the Table S1† and the calibration plot (Fig. 6d) for τ_1, τ_2, and τ_3 has been attained by following the equation:[66]

$$\frac{\tau_0}{\tau} = 1 + K_q\tau_0[Q] = 1 + K_D[Q] \quad (5)$$

Here, K_q, τ_0, τ, K_D, and Q represent a bimolecular quenching constant, a lifetime of TE-CQDs without and with the addition of quencher and S–V constant, respectively. The evaluated value of K_D (~6.07×10^4 M) demonstrates that ~40 μM concentration of Fe^{3+} will be required for ~38% quenching of the FL of TE-CQDs. On the other hand, the value of $K_q \sim 10.022 \times 10^{13}$ M^{-1} s^{-1} predicts a highly sensitive and efficient selection of TE-CQDs towards the sensing of Fe^{3+}. Further, some other calculations have been done and displayed in Table S1.†

3.4. Sensing of Fe^{3+} by TE-CQDs in HBS

To check the feasibility of the present framework for the sensing of Fe^{3+} in real samples, different concentration levels of HBS have been added to the solution of TE-CQDs and analysed through the method as discussed earlier. It has been found that the FL quenching occurs similarly to the standard solution. The FL emission spectra of the HBS after standard addition along with the calibration graph, S–V plot (Fig. 7a and b), and modified S–V plot (Fig. S7†) have been analysed for quenching of TE-CQDs FL by Fe^{3+}. Moreover, the linearity of the proposed probe pertaining K_{S-V} as 7.5×10^3 M^{-1}, 8.7×10^3 M^{-1} with regression coefficient $R^2 = 0.99$ in both cases (standard solution and HBS) (Fig. S8a and S8b†) offers remarkable attention. It also suggests that there has been no singular difference between the standard solution and HBS Fe^{3+} sensing. A similar analysis has been made with the HBS sample 2 and displayed in ESI (Fig. S9†). On the other hand, the matrix interference has been found negligible at 100-time higher concentration of the HBS sample. To check the stability of the method, similar measurements have been done almost after a week to a month, and no substantial significant change has occurred. A brief discussion regarding the sensing of iron ions in the respective samples has been elaborated in Table S2.†

3.5. The mechanism for FL quenching

It is evident from FL emission spectra and TRPL spectra that the FL intensity has quenched remarkably with the addition of the quencher in the solution of TE-CQDs and decay lifetime also gets changed substantially. Accordingly, there has been a clear indication of FL quenching due to both types of quenching

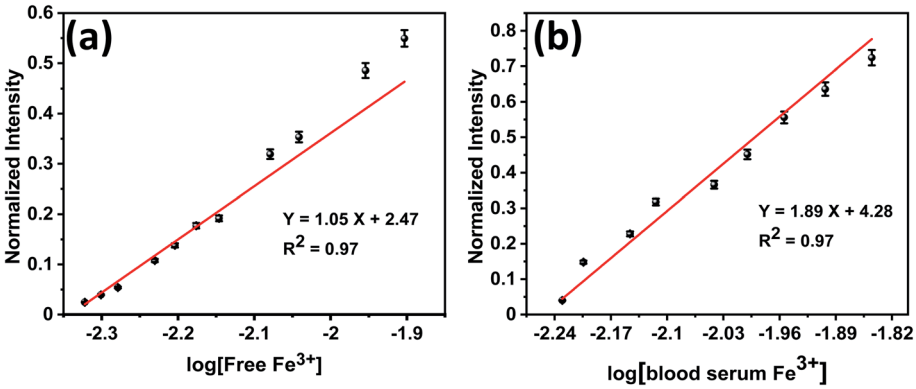

Fig. 9 Normalized FL intensity *vs.* log[concentration of quencher] plot for the detection of the LOD of the metal ion sensor in (a) standard solution and (b) HBS sample 1.

Table 1 Comparison of the CQDs FL quenching effect-based sensor with the earlier reported work for the metal ion (Fe^{3+}) sensing

Sensing probe	Linearity range (μM)	Limit of detection (μM)	K_{S-V} (M^{-1})	Matrix	References
Eu^{3+}:CDs@ZIF-8	0–6	0.89	—	Standard solution	70
CDs	8–80	3.8	—	Standard solution	71
NCQDs	0–70	0.50	—	Tap water, river water	72
CDs	33–133	0.53	1.62×10^3	Tap water, groundwater	73
Phe-CDs	5–500	0.72	—	Tap water	74
CQDs@OMS	25–750	—	—	Standard solution	75
TE-CQDs	0–90	0.37	7.5×10^3	**Standard solution**	**Present work**
TE-CQDs	0–70	0.36	8.7×10^3	**Human blood serum**	**Present work**

processes-collisional, and static. This could be due to the presence of various functional groups over the surface of the as-synthesized TE-CQDs. FT-IR measurements reveal the presence of COOH, OH, N–H, CH_2 electron-rich groups in the colloidal solution of TE-CQDs, and can efficiently attach with Fe^{3+}.[5,67] It has also been known that Fe^{3+} has significant potential to quench the FL by energy or electron transfer from an excited state to its 3d orbital owing to its paramagnetic behaviour.[3,68] A schematic illustration has been shown in Fig. 8 for both types of quenching. The complex formed in the excited state and ground state when get de-excited gives FL and No-FL,[66] respectively. Hence, FL of as-synthesized TE-CQDs gets quenched with the gradual addition of Fe^{3+}.

3.6. Limit of detection

The LOD has been calculated based on the FL titration measurements. Fig. 9 represents the variation of normalized FL intensity of TE-CQDs and log[concentration of quencher].[69] The present study possesses a good LOD as 0.37 μM and 0.36 μM in DI water (Fig. 9a) and HBS sample 1 (Fig. 9b), respectively, and have found to be comparable to other reported works (Table 1) and permissible in the frame of the guidelines of USEPA.

4. Conclusion

In summary, TE-CQDs have been successfully synthesized from TE as a natural precursor *via* hydrothermal treatment, without using any strong reducing additive and tedious post-cure, as a facile and cost-effective approach and subsequently studied the bio-sensing behavior for Fe(III). The as-synthesized TE-CQDs have been characterized by Raman, XRD, TEM, EDX, and XPS for their structural and elemental characterizations. Further, the photophysical properties of TE-CQDs have been investigated by UV-Visible and FL spectroscopy. The synthesized TE-CQDs are highly selective and exhibit remarkable sensing behavior to Fe^{3+}. Quenching constant K_a has a value ~4.24×10^3 M^{-1} which is almost 6.5% of the collision quenching phenomena derived constant and suggests a defined way of quenching by the quencher towards the TE-CQDs FL intensity, as unveiled by modified S–V plot. TRPL studies suggest the high selectivity ($K_q \sim 10.022 \times 10^{13}$ M^{-1} s^{-1}) and sensitivity of the TE-CQDs towards the Fe^{3+} sensing. The developed probe has good LOD ~ 0.37 μM and 0.36 μM in standard solution (linearity range ~ 0–90 μM) and HBS (linearity range ~0–70 μM), respectively. To the best of our knowledge, the present study inspects the synthesis of TE-derived CQDs, which is a cost-effective, eco-friendly approach for the very first time. Also, our findings unveil that the as-synthesized TE-CQDs can be used as an efficient, reliable, and feasible biosensor for sensing Fe^{3+} in biological samples.

Conflicts of interest

Authors have no conflicts to declare.

Acknowledgements

Pinky Sagar is thankful to DST, New Delhi for providing INSPIRE Fellowship (DST/INSPIRE/03/2018/000041). Dr Monika Srivastava acknowledges DST, New Delhi (SR/WOS-A/CS-52/2018) for WOS fellowship. The authors are thankful to the Bio-Physics Lab, Department of Physics, BHU Varanasi for the availability of different kinds of characterization facilities including FT-IR, UV-Visible, photoluminescence, and TRPL. Authors also convey their thanks to CIF, IIT BHU Varanasi for the access to characterization services.

References

1 G. M. Rodgers and J. A. Gilreath, *Acta Haematol.*, 2019, **142**, 13–20.
2 S. Gómez-Ramírez, E. Bisbe, A. Shander, D. R. Spahn and M. Muñoz, *Acta Haematol.*, 2019, **142**, 21–29.
3 B. Xue, Y. Yang, R. Tang, Y. Sun, S. Sun, X. Cao, P. Li, Z. Zhang and X. Li, *Cellulose*, 2020, **27**, 729–742.
4 G. Kalaiyarasan, J. Joseph and P. Kumar, *ACS Omega*, 2020, **5**, 22278–22288.
5 S. H. K. Yap, K. K. Chan, G. Zhang, S. C. Tjin and K.-T. Yong, *ACS Appl. Mater. Interfaces*, 2019, **11**, 28546–28553.
6 S. Dev and J. L. Babitt, *Hemodial. Int.*, 2017, **21**, S6–S20.
7 T. Arumugham, M. Alagumuthu, R. G. Amimodu, S. Munusamy and S. K. Iyer, *Sustainable Mater. Technol.*, 2020, **23**, e00138.
8 F. Liu, S. Zhu, D. Li, G. Chen and S.-H. Ho, *iScience*, 2020, **23**, 101174.
9 L. J. Mohammed and K. M. Omer, *Sci. Rep.*, 2020, **10**, 1–12.
10 G. Kalaiyarasan, M. Veerapandian, G. JebaMercy, K. Balamurugan and J. Joseph, *ACS Biomater. Sci. Eng.*, 2019, **5**, 3089–3099.
11 S. Y. Lim, W. Shen and Z. Gao, *Chem. Soc. Rev.*, 2015, **44**, 362–381.
12 Y. Wang and A. Hu, *J. Mater. Chem. C*, 2014, **2**, 6921–6939.
13 Y. Xiong, J. Schneider, E. V. Ushakova and A. L. Rogach, *Nano Today*, 2018, **23**, 124–139.
14 M. Sabet and K. Mahdavi, *Appl. Surf. Sci.*, 2019, **463**, 283–291.
15 S. Duraisamy, T. Suppan, K. Mohanta, M. Krishnamoorthy and B. G. Priyadarshini, *Nanotechnology*, 2020, **31**, 235401.
16 R. Das, R. Bandyopadhyay and P. Pramanik, *Mater. Today Chem.*, 2018, **8**, 96–109.
17 S. Panda, B. Paital and S. Mohapatra, *Colloids Surf., A*, 2020, 124445.
18 Y. Choi, N. Thongsai, A. Chae, S. Jo, E. B. Kang, P. Paoprasert, S. Y. Park and I. In, *J. Ind. Eng. Chem.*, 2017, **47**, 329–335.
19 X. Li, J. Chang, F. Xu, X. Wang, Y. Lang, Z. Gao, D. Wu and K. Jiang, *Res. Chem. Intermed.*, 2015, **41**, 813–819.
20 Y. Dong, R. Wang, G. Li, C. Chen, Y. Chi and G. Chen, *Anal. Chem.*, 2012, **84**, 6220–6224.
21 W.-B. Wu, Y.-C. Wong, Z.-K. Tan and J. Wu, *Catal. Sci. Technol.*, 2018, **8**, 4257–4263.
22 I. Kaminska, W. Qi, A. Barras, J. Sobczak, J. Niedziolka-Jonsson, P. Woisel, J. Lyskawa, W. Laure, M. Opallo and M. Li, *Chem.–Eur. J.*, 2013, **19**, 8673–8678.
23 J. Chen, M. Liu, Q. Huang, L. Huang, H. Huang, F. Deng, Y. Wen, J. Tian, X. Zhang and Y. Wei, *Chem. Eng. J.*, 2018, **337**, 82–90.
24 Y. Liu, W. Hou, H. Sun, C. Cui, L. Zhang, Y. Jiang, Y. Wu, Y. Wang, J. Li and B. S. Sumerlin, *Chem. Sci.*, 2017, **8**, 6182–6187.
25 R. Jiang, M. Liu, T. Chen, H. Huang, Q. Huang, J. Tian, Y. Wen, Q.-y. Cao, X. Zhang and Y. Wei, *Dyes Pigm.*, 2018, **148**, 52–60.
26 T. Li, L. Xie, R. Long, C. Tong, Y. Guo, X. Tong, S. Shi and Q. Lin, *Microchim. Acta*, 2019, **186**, 791.
27 Y. Yan, C. Zhang, W. Gu, C. Ding, X. Li and Y. Xian, *J. Phys. Chem. C*, 2016, **120**, 12170–12177.
28 J. B. Essner, J. A. Kist, L. Polo-Parada and G. A. Baker, *Chem. Mater.*, 2018, **30**, 1878–1887.
29 H.-c. Tan, W.-h. Zhao, Q. Qiu, R. Zhang, Y.-y. Zuo and L.-j. Yang, *Fullerenes, Nanotubes, Carbon Nanostruct.*, 2017, **25**, 417–422.
30 G. Yang, X. Wan, Y. Su, X. Zeng and J. Tang, *J. Mater. Chem. A*, 2016, **4**, 12841–12849.
31 F. Abdolrezaei and M. Sabet, *Luminescence*, 2020, **35**, 684–693.
32 R.-C. Wang, J.-T. Lu and Y.-C. Lin, *J. Alloys Compd.*, 2020, **813**, 152201.
33 J. Zheng, Y. Xie, Y. Wei, Y. Yang, X. Liu, Y. Chen and B. Xu, *Nanomaterials*, 2020, **10**, 82.
34 W. Wang, Z. Wang, J. Liu, Y. Peng, X. Yu, W. Wang, Z. Zhang and L. Sun, *Ind. Eng. Chem. Res.*, 2018, **57**, 9144–9150.
35 M. Lu, Y. Duan, Y. Song, J. Tan and L. Zhou, *J. Mol. Liq.*, 2018, **269**, 766–774.
36 Q. Liang, W. Ma, Y. Shi, Z. Li and X. Yang, *Carbon*, 2013, **60**, 421–428.
37 T. Wang, X. Liu, C. Ma, Z. Zhu, Y. Liu, Z. Liu, M. Wei, X. Zhao, H. Dong and P. Huo, *J. Alloys Compd.*, 2018, **752**, 106–114.
38 H. Xu, L. Xie and M. Hakkarainen, *ACS Sustainable Chem. Eng.*, 2017, **5**, 5360–5367.
39 N. Chaudhary, P. K. Gupta, S. Eremin and P. R. Solanki, *J. Environ. Chem. Eng.*, 2020, **8**, 103720.
40 A. A. Safar, A. O. Ghafoor and D. Dastan, *Pol. J. Environ. Stud.*, 2020, **29**, 2317–2326.
41 O. Vallisuta, V. Nukoolkarn, A. Mitrevej, N. Sarisuta, P. Leelapornpisid, A. Phrutivorapongkul and N. Sinchaipanid, *Exp. Ther. Med.*, 2014, **7**, 246–250.
42 J. Shetty, H. Harikiran and J. Fernandes, *J. Pharm. Res.*, 2009, **2**, 1035–1038.
43 T. M. Madanan, I. K. Shah, G. K. Varghese and R. K. Kaushal, *Environ. Chem. Ecotoxicol.*, 2021, **3**, 17–22.
44 A. Maji, M. Beg, S. Das, M. N. Aktara, S. Nayim, A. Patra, M. M. Islam and M. Hossain, *Process Biochem.*, 2020, **97**, 191–200.
45 S. Suzen, H. Gurer-Orhan and L. Saso, *Molecules*, 2017, **22**, 181.
46 Q. Fan, J. Li, J. Wang, Z. Yang, T. Shen, Y. Guo, L. Wang, M. S. Irshad, T. Mei and X. Wang, *J. Mater. Chem. C*, 2020, **8**, 4685–4689.

47 K. K. Jinadasa, P. Herbello-Hermelo, E. Peña-Vázquez, P. Bermejo-Barrera and A. Moreda-Piñeiro, *Talanta*, 2021, **224**, 121841.
48 B. B. Yıldırmaz, A. Gölcü, B. T. Zaman, N. A. Kasa, E. G. Bakırdere and S. Bakırdere, *Chem. Pap.*, 2021, 1–8.
49 J. H. Yoe and A. L. Jones, *Ind. Eng. Chem., Anal. Ed.*, 1944, **16**, 111–115.
50 S. Li, C. Zhang, S. Wang, Q. Liu, H. Feng, X. Ma and J. Guo, *Analyst*, 2018, **143**, 4230–4246.
51 K. P. Carter, A. M. Young and A. E. Palmer, *Chem. Rev.*, 2014, **114**, 4564–4601.
52 Z. Qian, J. Ma, X. Shan, H. Feng, L. Shao and J. Chen, *Chem.–Eur. J.*, 2014, **20**, 2254–2263.
53 R. Wang, K.-Q. Lu, Z.-R. Tang and Y.-J. Xu, *J. Mater. Chem. A*, 2017, **5**, 3717–3734.
54 K. Dave and V. G. Gomes, *Nano Energy*, 2019, 104093.
55 S. Yang, W. Yue, D. Huang, C. Chen, H. Lin and X. Yang, *RSC Adv.*, 2012, **2**, 8827–8832.
56 X. Feng and Y. Zhang, *RSC Adv.*, 2019, **9**, 33789–33793.
57 G. Li, M. Pei and P. Liu, *Mater. Sci. Eng. C*, 2020, 110653.
58 S. K. Srivastava, P. Sagar, M. Srivastava and R. Prakash, *Anal. Methods*, 2020, **12**, 3014–3024.
59 V. Sharma, A. K. Saini and S. M. Mobin, *J. Mater. Chem. B*, 2016, **4**, 2466–2476.
60 S. Muthulingam, I.-H. Lee and P. Uthirakumar, *J. Colloid Interface Sci.*, 2015, **455**, 101–109.
61 Y.-L. Zhang, L. Wang, H.-C. Zhang, Y. Liu, H.-Y. Wang, Z.-H. Kang and S.-T. Lee, *RSC Adv.*, 2013, **3**, 3733–3738.
62 S. Bansal, J. Singh, U. Kumari, I. P. Kaur, R. P. Barnwal, R. Kumar, S. Singh, G. Singh and M. Chatterjee, *Int. J. Nanomed.*, 2019, **14**, 809.
63 H. Wu, L.-F. Pang, M.-J. Fu, X.-F. Guo and H. Wang, *J. Pharm. Biomed. Anal.*, 2020, **180**, 113052.
64 J. Zhu, H. Chu, T. Wang, C. Wang and Y. Wei, *Microchem. J.*, 2020, **158**, 105142.
65 L. Chunduri, A. Kurdekar, S. Patnaik, B. V. Dev, T. M. Rattan and V. Kamisetti, *Mater. Focus*, 2016, **5**, 55–61.
66 J. R. Lakowicz, *Principles of fluorescence spectroscopy*, Springer Science & Business Media, 2013.
67 M. A. Issa, Z. Z. Abidin, S. Sobri, S. A. Rashid, M. A. Mahdi and N. A. Ibrahim, *Sci. Rep.*, 2020, **10**, 11710.
68 J. Li, Q. Wang, Z. Guo, H. Ma, Y. Zhang, B. Wang, D. Bin and Q. Wei, *Sci. Rep.*, 2016, **6**, 1–8.
69 M. Shortreed, R. Kopelman, M. Kuhn and B. Hoyland, *Anal. Chem.*, 1996, **68**, 1414–1418.
70 X. Guo, Q. Pan, X. Song, Q. Guo, S. Zhou, J. Qiu and G. Dong, *J. Am. Ceram. Soc.*, 2021, **104**, 886–895.
71 Y. Chen, X. Sun, W. Pan, G. Yu and J. Wang, *Front. Chem.*, 2020, **7**, 911.
72 J. Zhu, H. Chu, T. Wang, C. Wang and Y. Wei, *Microchem. J.*, 2020, 105142.
73 A. M. Senol and E. Bozkurt, *Microchem. J.*, 2020, **159**, 105357.
74 Z.-F. Pu, Q.-L. Wen, Y.-J. Yang, X.-M. Cui, J. Ling, P. Liu and Q.-E. Cao, *Spectrochim. Acta, Part A*, 2020, **229**, 117944.
75 Y. Dong, J. Ma, C. Liu and Y. Bao, *Ceram. Int.*, 2020, **46**, 11115–11123.